NDT&E International 132 (2022) 102731

Contents lists available at ScienceDirect

NDT and E International

journal homepage: www.elsevier.com/locate/ndteint

Thermosonic inspection of carbon fibre reinforced polymer composites using an airborne haptic ultrasonic phased array

R.L. Watson [a], D.R. Billson [b], D.A. Hutchins [b], F. Ciampa [a,*]

[a] Department of Mechanical Engineering Sciences, University of Surrey, Guildford, Surrey, GU2 7XH, UK
[b] School of Engineering, University of Warwick, Coventry, CV4 7AL, UK

ARTICLE INFO

Keywords:
Non-destructive evaluation
Thermosonics
Ultrasonics
Infrared imaging
Composite materials
Phased array

ABSTRACT

This paper reports the development of a contactless non-destructive evaluation technique using an air-coupled haptic ultrasonic phased array to induce thermosonic frictional heating in damaged carbon fibre reinforced polymer composites. Haptic ultrasonic systems consist of controllable, narrowband, and high-power piezoelectric transducer arrays that are capable of electronically steering and shaping the ultrasonic beam on the surface of test samples. Localised thermal images of the damaged area were observed using an infrared camera. It was found that the intensity of the thermosonic heating reduced with increased distances between the ultrasonic excitation location and the damage. This approach allowed the ultrasonic focal point to be moved across the sample to identify the areas of damage, without moving either the array or the infrared camera, thus significantly decreasing the time needed for inspection.

1. Introduction

Carbon Fibre Reinforced Polymer (CFRP) composites make up today a significant proportion of modern aerospace structures, and their use is increasing in the automotive sector. The high stiffness and strength of CFRP materials coupled with weight savings and fatigue resistance are driving this increasing use. For example, the Boeing 787 Dreamliner uses composites to account for nearly 50% of the airframe weight [1], whereas the Airbus A350 XWB wing design is predominantly made from composites and the plane is 53% composite overall [2]. Use of composite materials in these safety-critical applications requires rigorous inspections for defects or damage to ensure safe operation. Non-Destructive Evaluation (NDE) of CFRP and composite materials in general is therefore essential, both during their production and when in service. Significant failures may occur from manufacturing defects or damage sustained during service [3]. A wide number of types of damage of interest in composites includes low velocity impacts, high velocity impacts, static overload, fatigue, moisture ingress, lightning strikes or overheating [4]. One of the difficulties with impact damage in composites is that significant subsurface damage may be present with no visible or only barely visible surface damage present. This requires assessment of the entire volume of the composite to ensure it is safe for use. It is thus essential that NDE methods are available to detect such defects, both for reasons of safety and for reducing the downtime of a component or structure. Development of techniques which allow rapid in-situ examination and assessment of composite structures in a wide variety of industries would be very useful.

A wide range of NDE techniques are in used for the assessment of composite materials, including acoustic emission, ultrasonics (both linear and nonlinear), digital image correlation, x-ray radiography, and infrared (IR) thermography [5,6]. However, these methods tend to require either continuous monitoring of a structure or removal of the parts for inspection. Automated techniques exist that scan newly manufactured pieces such as wing spars in ultrasonic immersion baths for defects, and wings can be inspected using rolling contact or water immersion systems whilst still in the production facility. Conventional ultrasonic testing using contact arrays and a couplant is a widely used procedure for imaging composite structures, but requires multiple test locations to investigate a large component. Air-coupled ultrasonic scanning overcomes the need for water immersion or the use of couplant [7], but is limited by acoustic impedance mismatch at the air/sample boundary and the significant loss of energy at the interface.

Current ultrasonic inspection methods use linear ultrasound with the system either in a send/receive mode with two transducers arrangement, or a pitch-catch with a single transducer looking at reflections to identify when damage is present. These linear operations analyse the

* Corresponding author.
E-mail address: f.ciampa@surrey.ac.uk (F. Ciampa).

https://doi.org/10.1016/j.ndteint.2022.102731
Received 4 June 2022; Received in revised form 28 July 2022; Accepted 24 August 2022
Available online 3 September 2022

difference between the received signal and the one which was sent to look for ultrasonic changes indicative of any damage. The signal from small amounts of damage in linear ultrasound is typically small in relation to the transmitted signal. This makes it a challenge to detect and identify the damage. For this reason, nonlinear ultrasound has an advantage in some situation where a signal at a different frequency is detected due to nonlinearity at the defect [8]. Nonlinear ultrasonics has been suggested as an approach that could be useful in some situations for the detection of damage in composites [9]. One limiting factor in many inspections is the need for couplant [8], which has been shown to impact on the accuracy of some measurements [10–13]. Removing the need for contact with the surface would thus be of advantage.

For these reasons, researchers have been investigating other techniques for the inspection of composites. One of these is thermography [14], which is an inherently rapid process with the ability to test large areas investigated in a single measurement without disassembly or contact with the surface. Traditional thermography works by applying heat to objects under study and measuring the heat propagation through the samples using an IR camera [14]. Defects can modify heat conduction, so that damaged areas can be identified. It is known, however, that orientation of defects and their in-depth location influence detectability [15].

An alternative approach is thermosonics, which uses the nonlinear response of damaged material to the applied ultrasonic excitation to generate frictional heat at damage interfaces. Such heat can then be detected via IR imaging cameras as a change in the surface temperature. Thermosonics has been shown to detect defects which may not be found by traditional thermography, especially if the defect has only a minor effect on heat flow [16,17]. The self-heating of the damaged area in thermosonics allows rapid identification of the location of damage and allows for more detailed inspection by other routes if required [18]. Thermosonics has been used in previous work to monitor the efficacy of metal bonding [19] and to inspect aluminium components subject to fatigue loading [20], as well as electrical connections in silicon-based electronic substrates [21]. Thermosonics has also been used to inspect composites [22], e.g., by using mechanical vibration induced by a mechanical shaker to give amplitude modulated lock-in vibro-thermography [23]. Another common approach is the use of an ultrasonic horn to excite the sample [24,25]. Both approaches require the vibration source to be in contact with the sample surface.

The wave field generated by an ultrasonic horn - or any other contact-type mechanical excitation method - generates vibrations that at locations of damage result in nonlinear asynchronous motion on either side of a defect such as a crack. These asynchronous vibrations in the material result in a range of motion typically referred to as clapping, where the surfaces of the damage rub together and generate heat through friction [16]. This localised heating is what makes the technique so powerful, as only the damaged portion results in significant friction and localised heating. This localised response can also highlight damage which may not be visible due its orientation with traditional thermographic techniques. The selectivity of thermosonics as a NDE technique makes it an area of much interest in the safety-critical investigation of CFRP materials.

However, there is still the problem that contact is usually made to the sample by the ultrasound generation system. For this reason, the current authors have investigated a new air-coupled haptic ultrasonic excitation system for thermosonics. This removes the need for direct contact with the sample, allowing for a more rapid thermal inspection. The primary challenge with using airborne ultrasound for insonifying a sample is the poor efficiency of energy transfer between air and the solid material. This is dependent upon the relative differences between the acoustic impedance of air and that of the composite. Zalameda et al. [26] proposed the use of air-coupled acoustic signals at frequencies of up to 2 kHz and at very high intensities (105 dBA) and were able to observe thermosonic effects in composite core materials. This very high level of incident sound intensity would, however, not be necessary if a higher ultrasonic frequency was used that was able to generate localised thermosonic clapping, especially if it could be localised and scanned over the sample. Solodov et al. [27] have shown both modelling and experimental results to determine local defect resonance frequencies of machined flat-bottomed holes in polymers. This use of modelling to predict local defect resonance frequencies allowed the use of lower energy air-coupled ultrasound to observe thermosonic effects with transducers centred around the resonance frequency.

This paper describes an approach whereby piezoelectric air-coupled arrays are used as the excitation of composite CFRP samples. These arrays use a set of resonant piezoelectric 40 kHz transducers as ultrasonic sources, from which focussed and narrowband high energy excitation can be generated, thus reducing the problem caused by the high reflectivity at the air/sample interface. Use of these phased ultrasonic arrays allows the focussed excitation to be electronically controlled including swept over the sample surface and the intensity and modulation varied, while the arrays themselves remain stationary, speeding up the process of sample examination. Such arrays have been developed for use in haptics, which is concerned with the generation of artificial touch sensations through the application of forces or vibration [28]. The use of an array to produce a mid-air tactile response was first presented by Iwamoto et al. [29], who showed that phase delays between array elements could be used to focus their array. Hoshi et al. [30] also used this approach to control the position of the focal point in 3D space using constructive interference. Note that ultrasonic arrays for use in air have also been reported at low amplitudes, for use in various activities such as imaging, levitation, particle manipulation and other applications, [31–34].

This applied excitation will generate a normal force at the surface at the focal point on the surface of the sample. Depending on the size of the focal region and the excitation frequency, a range of elastic modes can be generated in the composite sample (assumed here to be in the form of a parallel-sided thin plate). Predominantly these are likely to be both longitudinal waves that travel through the thickness of the sample and guided waves (e.g., the A0 Lamb wave mode) that will radiate laterally away from the source. Longitudinal waves are likely to be most efficiently generated by the focused air-coupled excitation source, provided it is thick enough to support them, although shear waves and other guided wave modes could also be generated at lower efficiencies. It would be expected that the induced vibrations will be of greatest magnitude at the location of the focal region of the array – even for guided waves this would be the case. In the experiments to be described here, the A0 Lamb mode is most likely to be generated, as the plate thickness was much less than the wavelength of longitudinal waves in the composite material. This localized reaction, and the scanning of the focal point of the array across the sample surface, would allow multiple rapid thermosonic measurements to be made in a single experiment. This increase in speed of measurement, without the need to relocate equipment, could make this a suitable system for a wide range of non-contact NDE measurements.

2. Experiment

Samples of 3 mm thick CFRP composite plates of 250 mm by 230 mm size were obtained from Easy Composites (Stoke on Trent, United Kingdom). Each sample had one side with a gloss finish the other as a peel-ply matte. The peel-ply matte side was used for infrared detection of thermosonically-induced temperature rises to avoid the presence of unwanted reflected light from ambient sources [Fig. 1(a)]. Ultrasonic excitation was also on the same side of the sample. This is an important point – most NDE inspections are needed as single-sided measurements, as access to both sides is often not possible. One of the sheets [Fig. 1(b)] was damaged using a 13.5 mm ball bearing and a manual hydraulic press, so that ball bearing travelled 6.75 mm (the radius) compressing and deforming the sample against a soft support structure causing visible damage on the matte surface, the deformed surface was then

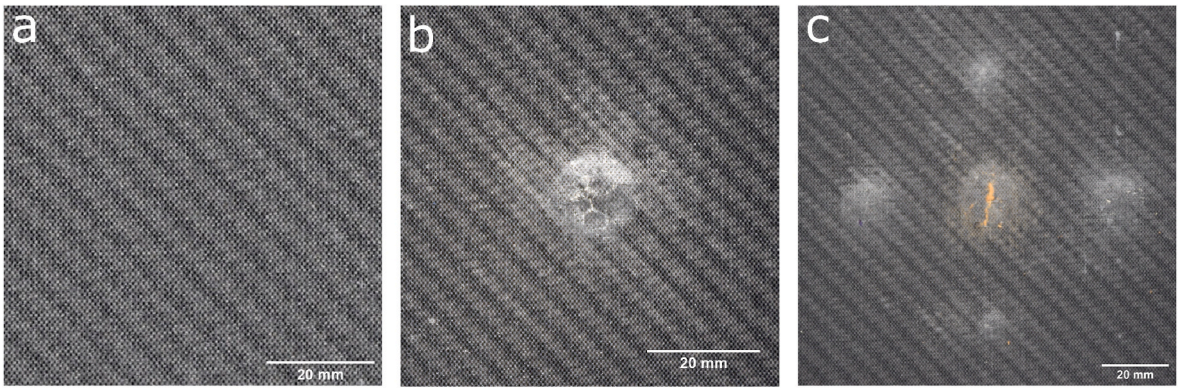

Fig. 1. Surface photographs of CFRP samples (a) as received, (b) after the introduction of a single point of damage, and (c) after the introduction of five points of damage plate. These are the matte side of the CFRP samples; the ball bearings used to case the damage acted on the other (gloss) side of the sample.

pressed back to flat. Another sample [Fig. 1(c)] was damaged with a range of ball bearing sizes (13.5, 12, 10, 8 and 6 mm) in the same way. The multiple damage locations were placed approximately 40 mm from the centre. Photographs of the damage on the matte surface are shown both before and after damage was introduced in Fig. 1.

The apparatus is shown schematically in Fig. 2(a), and the ultrasonic source used in these experiments (an Ultrahaptics Stratos Explore ultrasonic array) is shown in Fig. 2(b). Fig. 3 is a photograph of the experimental set up, with a CFRP composite plate containing damage shown in situ on a foam cushioning layer.

This ultrasonic array generated a powerful focused ultrasound response, having been designed originally for use in haptic systems. It consisted of an array of 256 (16 × 16) by 167 mm square piezoelectric airborne transducers operating at an excitation frequency of 40 kHz. The array was controlled by software which allowed the ultrasonic beam to operate with a focal spot at multiple point on the sample surface which was situated at a distance of 300 mm from the array. The 40 kHz signal produced by the array could be adjusted in both intensity and modulation, and in our case was a signal with a duty cycle of 200/100 ms on/off which was repeated for the duration of the excitation period. The strongly pulsed nature was used to locally excite the sample through the thickness. As mentioned earlier, A0 mode Lamb waves would be the most likely elastic mode to have been generated, but the measurements focussed on locally exciting specific regions of the composite surface, so to observe any thermosonic local increase in temperature from the presence of damage at that location (and where the A0 amplitude would be at its highest before dissipating laterally along the composite plate). The advantages that this array were (i) the high intensity ultrasonic output and (ii) the fact that the focal point of the ultrasound could be moved in a programmable manner. This ability to move the focal point allowed scanning of the thermosonic excitation across the sample. High intensity ultrasound results in general vibration in the sample and of the

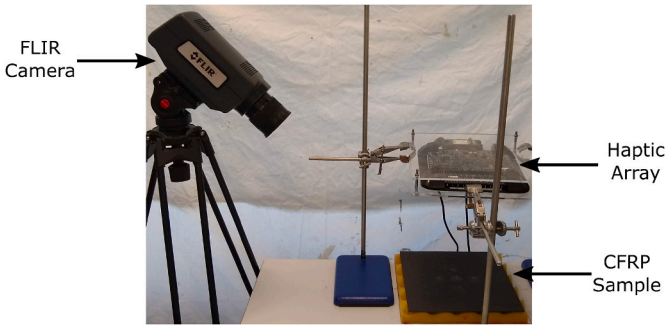

Fig. 3. Photograph of the experimental apparatus.

defect, the two sides of the defect react differently to the vibration resulting in rubbing and friction generating local heating. Excitation scanned across the sample through control of the array allows a range of points on a sample under inspection to be inspected without moving either the apparatus or the sample.

Infrared imaging was carried out with an FLIR A6571 camera with an Indium Antimonide sensor producing a 640 × 512 pixel image with a spectral range of 3–5 μm, a thermal sensitivity of 20 mK, and the capacity to record data at rates of up to 125 Hz. It was able to detect the temperature changes of over 0.05 °C due to thermosonic heating. In the work presented here, image capture was undertaken at 10 Hz over longer time periods to record the ultrasonically induced heating on the matte sample surface, as shown in Fig. 2(a). Research IR software (Teledyne FLIR LLC, Wilsonville, Oregon, USA) was used to initially view the results and to output images and movies of the recorded frames. Subsequent processing with Matlab highlighted the changes in temperature that occurred during ultrasonic excitation. The temperature of

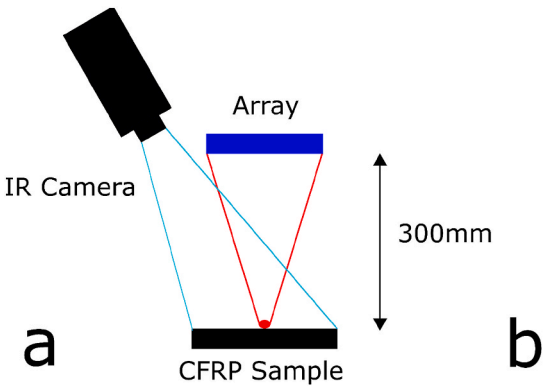

Fig. 2. (a) Diagram showing the set-up of the array and infrared camera to undertake thermosonic measurements. The 300 mm separation between the array and the CFRP composite plate is to ensure that the required angle of the infrared camera allows measurement of the entire surface of the sample to take place. (b) Photograph of the Ultrahaptics Stratos Explore array used in this work. The image shows the array in a frame to allow it to be held above samples without obscuring any of the array elements. The active area of the array was 167 mm × 167 mm.

each pixel in the image at the start of the ultrasonic excitation was subtracted from the corresponding pixel in all subsequent frames, providing a measure of the changes in temperature during excitation. This processing showed clear local heating during excitation. Upon ceasing excitation, the local heating at the excitation site was observed to decrease, gradually returning to the surrounding CFRP temperature. Thermosonics results were recorded using a standard procedure using a "clapper board" in the form of a warm object passed in front of the lens to indicate the start of the experiment. Excitation with ultrasound from the haptic array then took place over a 20–30 s time duration, so as to allow sufficient time for local heating to be observed. The 'clapper board' was then passed in front of the lens a second time, and the incident ultrasonic signal was then switched off. IR data was then collected for another 10–40 s to record the cooling of the sample before the recording was stopped. The main ultrasonic output of the array was limited to 40 kHz due to the array being composed of piezoelectric airbourne transducers. The piezoelectric elements are resonant and their dimensions control their principal emission frequency. With this resonance-based property, harmonics are also generated. Fig. 4 shows the results from a measurement taken in air, where the 40 kHz principal frequency as well as the second and third harmonics at 80 kHz and 120 kHz respectively can be observed. The power from the array was measured with a Bruel and Kjaer calibrated ultrasonic sensitive microphone and found to be a linear response to variation in the power setting and determined to be 68.9 Pa at 100%.

3. Results and discussion

For an undamaged sample, application of the 40 kHz signal with the 200 ms/100 ms on/off duty cycle for a 25 s exposure resulted in the image shown in Fig. 5(a). Note that the temperature values of each pixel in the frame had the initial temperature subtracted from them to show localised heating. It can be observed that there was no obvious effect, with a reasonably uniform temperature profile throughout. Without any damage to allow clapping at the surfaces of the damage to occur, no localised thermosonically generated heating was observed. With the damaged sample containing only one defect [Fig. 5(b)], heating was then observed directly, with the array focussed on the damage. With the sample containing five defects, the sample was excited at the central defect, but localised heating at the other four regions of damage can be observed in Fig. 5(c). This indicates that a response is also being observed at some distance from the focal spot region, but only where

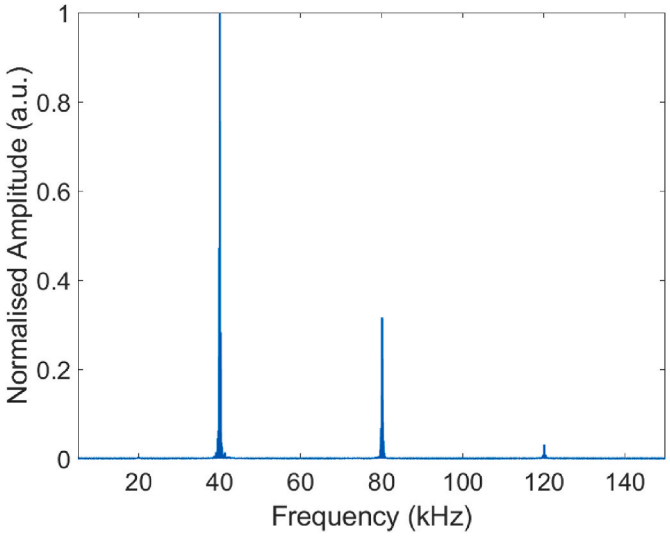

Fig. 4. Normalized frequency spectra output of the array. The 40 kHz driving frequency is accompanied by the second and third harmonics at 80 kHz and 120 kHz.

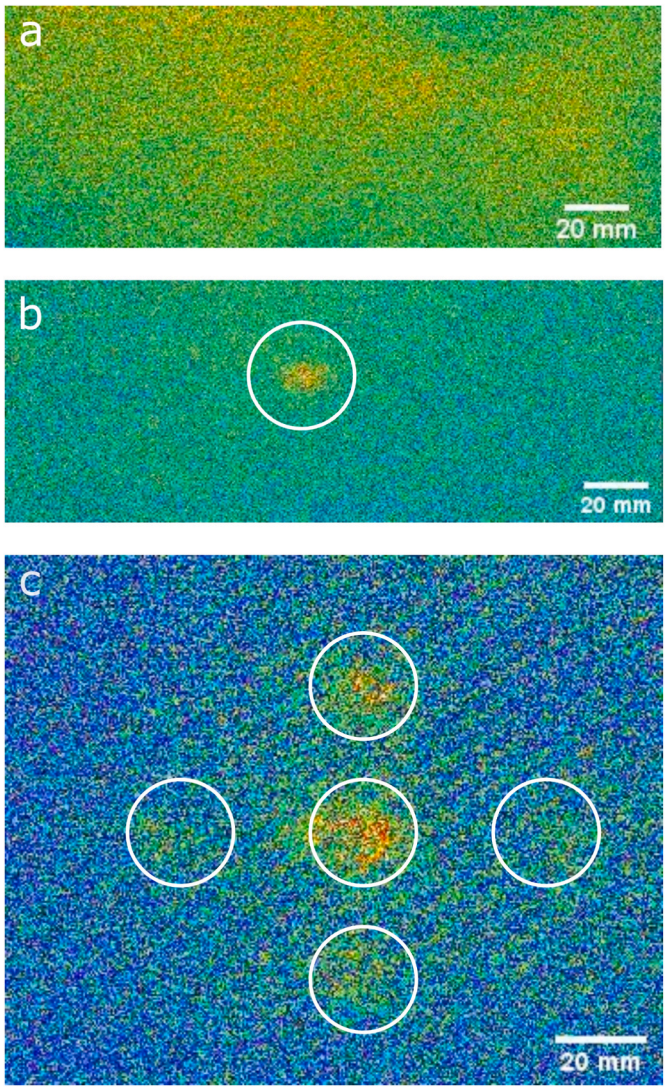

Fig. 5. (a) Thermosonic image of the undamaged sample subjected to pulsed excitation. No local heating was observed with undamaged samples. (b) As in (a), but now the focal spot was applied at the location of the single defect for the sample with one defect only. The thermosonically-generated heated location has been highlighted by a white ring. (c) Results for the sample with 5 defects, but with the focal spot located above the central one.

there was a defect. Note that in all three cases, removal of the ultrasonic stimulation led to cooling of the samples back to ambient temperatures.

Fig. 5(a) confirms that thermosonic heating was not due to general local heating of the CFRP substrate at the point of excitation. The best excitation of a detectable IR signature and a temperature rise at the surface was shown to be when the focal spot was directly above the damage location – this was needed to induce the greatest degree of "clapping" of the defect surfaces at 40 kHz. Further, Fig. 5(b) seemed to indicate that little heating was detected at distances further away from the defect, as would be expected, when excitation was directly above it. To investigate this behaviour further, the focal region of the array was moved away from the area of damage on the sample containing only one defect. These results are shown in Fig. 6, where two different locations of the array focal point on the sample surface is identified by the black spots, both being at some distance from the known defect location. The signature of the defect is visible in both cases but is much weaker than when the focal spot was directly above the defect.

Fig. 7 shows the apparent temperature difference of individual pixels over the duration of ultrasonic excitation. The apparent temperature as

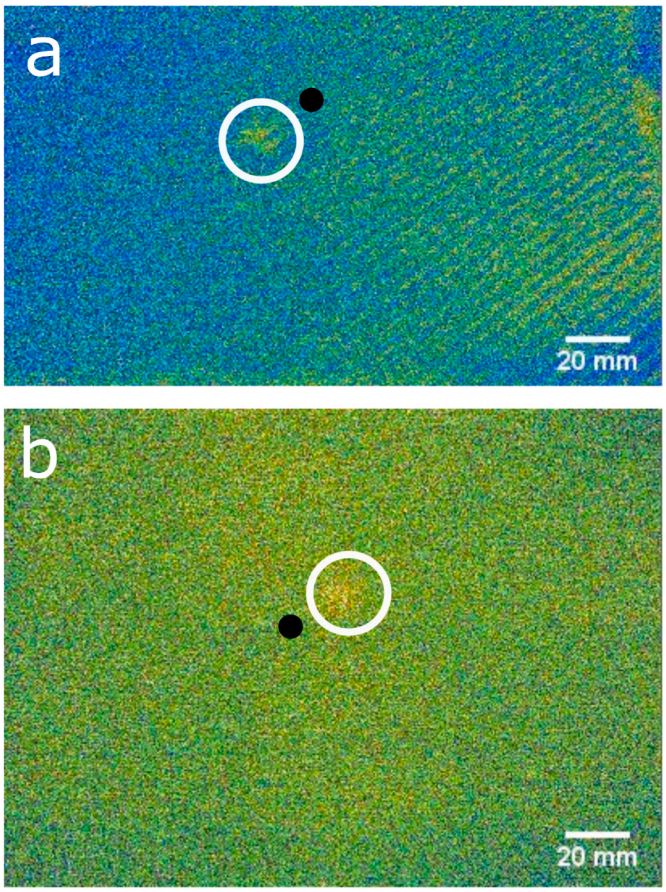

Fig. 6. Demonstration of a weaker thermosonic signature when the excitation was not directly at the defect location. The array focal point of excitation is indicated by the black spot in each case. The resulting thermosonic heating is highlighted within the white ring. The excitation was moved diagonally (a) up and right and (b) diagonally down and left from location of the defect.

measured by the IR camera will be affected by differences in emissivity across the sample surface. To overcome this variation, the difference from an initial apparent temperature measured at the start of ultrasonic excitation has been plotted. As it can be observed, the pixels with a 0.1 °C rise or greater are observed with the focal spot located at the defect location (blue trace), data from Fig. 5(b). The other two other traces that remain between 0 °C and – 0.05 °C were taken from Fig. 6(b). The first (dotted red line) shows a small rise in temperature at the defect location when the excitation was some distance away (the black spot). This shows that the array focal point was generating some small increase in surface temperature above the defect. The lower trace, measured at the black spot excitation location in Fig. 6(b), shows very little surface temperature increase with time, as would be expected. These temperature increases with time confirm that thermosonic heating requires the presence of damage, but also that it can be excited at some distance from the damage to produce defect signatures at the defect location.

To investigate the impact the power level from the array has upon the thermosonic response the power of the array was varied. Fig. 8 shows the increasing time taken to reach a maximum apparent temperature difference from excitation with lower power settings. The continued rise in apparent temperature difference with longer excitation times indicates that the length of excitation is another factor to be considered when further developing thermosonic techniques. The reduced power excitations were run for longer periods to determine if there was a time dependent element to the thermosonic heating during excitation. Shorter times were used with higher power as these provided adequate heating to identify the nature of thermosonic heating. The

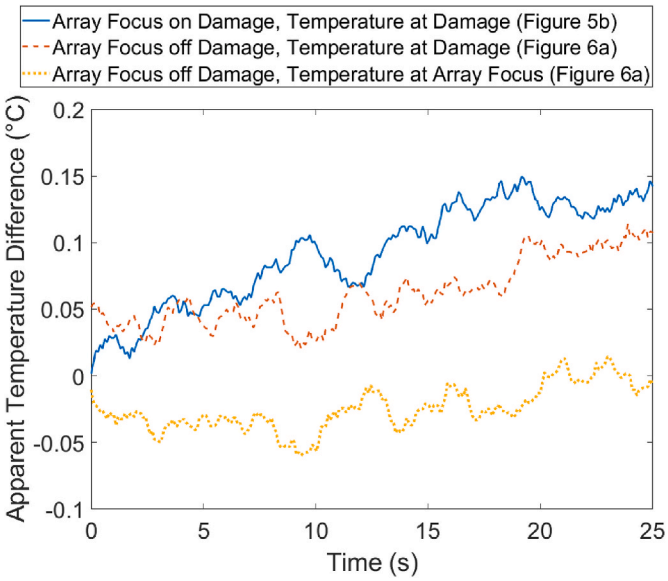

Fig. 7. Apparent temperature difference with time from starting ultrasonic excitation of the haptic array. This data is from the CFRP sample containing only one defect. These traces correspond to: blue solid line – the temperature measured above the defect and coincident with the excitation location [from Fig. 5(b)]; red dashed line – the temperature measured at the damage location (within the white circle of Fig. 6(a)) but with the array focused at the black spot; yellow dotted line – the temperature at the location of the focus of the array in Fig. 6(a). (For interpretation of the references to colour in this figure legend, the reader is referred to the Web version of this article.)

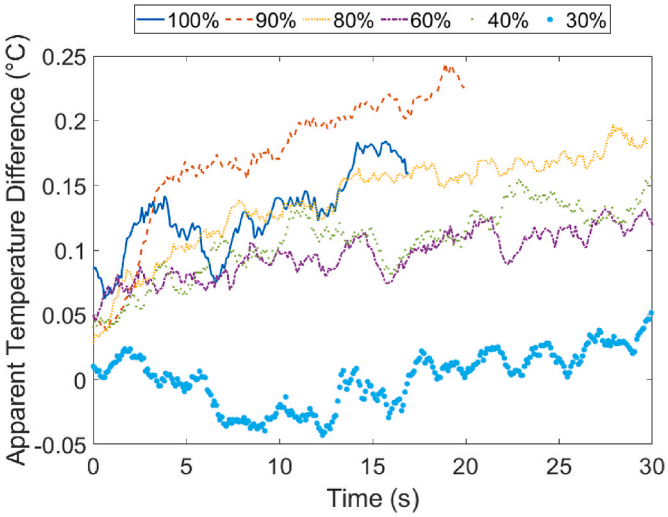

Fig. 8. The impact of array power level on the time and temperature change at the defect when focussed on the single 13.5 mm defect.

magnitude of the apparent temperature difference also decreases with lower applied power. All of these traces are from the same single pixel on the sample studied without moving the sample or equipment between experiments with the range of applied powers. It is interesting to note that the 100% (full power) setting produces a lower maximum apparent temperature difference than 90% but begins to heat up more rapidly. The difference between 60% and 40% has a similar trend with more rapid initial heating at higher power. At 30% applied power, it can be observed that no heating trend is visible and insufficient power has been applied generate a measurable thermosonic response. This level of power clearly shows that the point at which the excitation intensity is insufficient to generate clapping with a single frequency application at

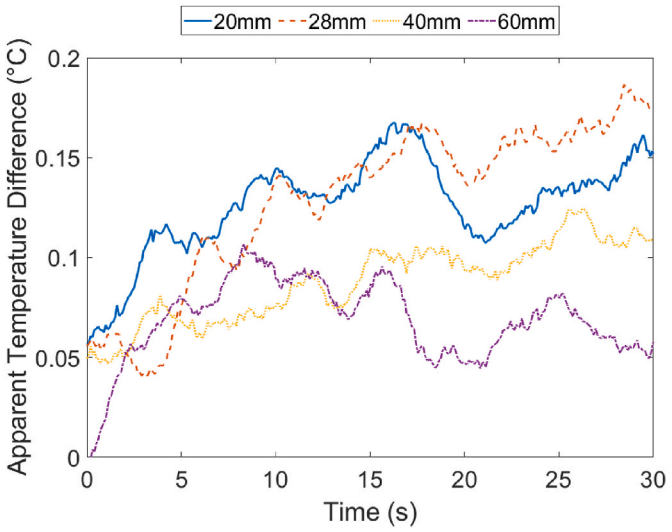

Fig. 9. The impact on temperature increase cause by moving the excitation focus away from the region of damage, and studying the temperature rise at the defect location.

40 kHz.

The level of thermosonic temperature increases directly above the damage area was now studied as the array focal spot was moved to known distances from the defect location, and the excitation switched on. This was undertaken at 100% power output from the array at distances of 20, 28, 40 and 60 mm. In general, temperature increases are greater for smaller distances of the focal region from the defect, as it might be expected.

The measurements at 20 and 28 mm are at a similar level to the 80% power result shown in Fig. 8. Note also that there was an approximately 20% power drop in the behaviour of the response for each 20 mm moved away from the damage. This diminution in the level of heating is to be expected. The energy travelling through the sample away from the array focus will decline due to the material properties. This reduction in energy arriving at the damage results in lower vibration levels and hence less induced heating through reduced clapping action within the damage. This lower intensity of heating in the area of excitation when at a distance to the focal point of the array is consistent with results from contact ultrasonic horn studies published by other authors [16,25]. The presence of a measurable thermosonic effect when the array was focused a distance away from an area of damage confirms that scanning of the array across a sample at predetermined intervals is likely to be a viable technique to investigate an unknown sample. A linear scan through the defect, for example, would excite the defects present both within the

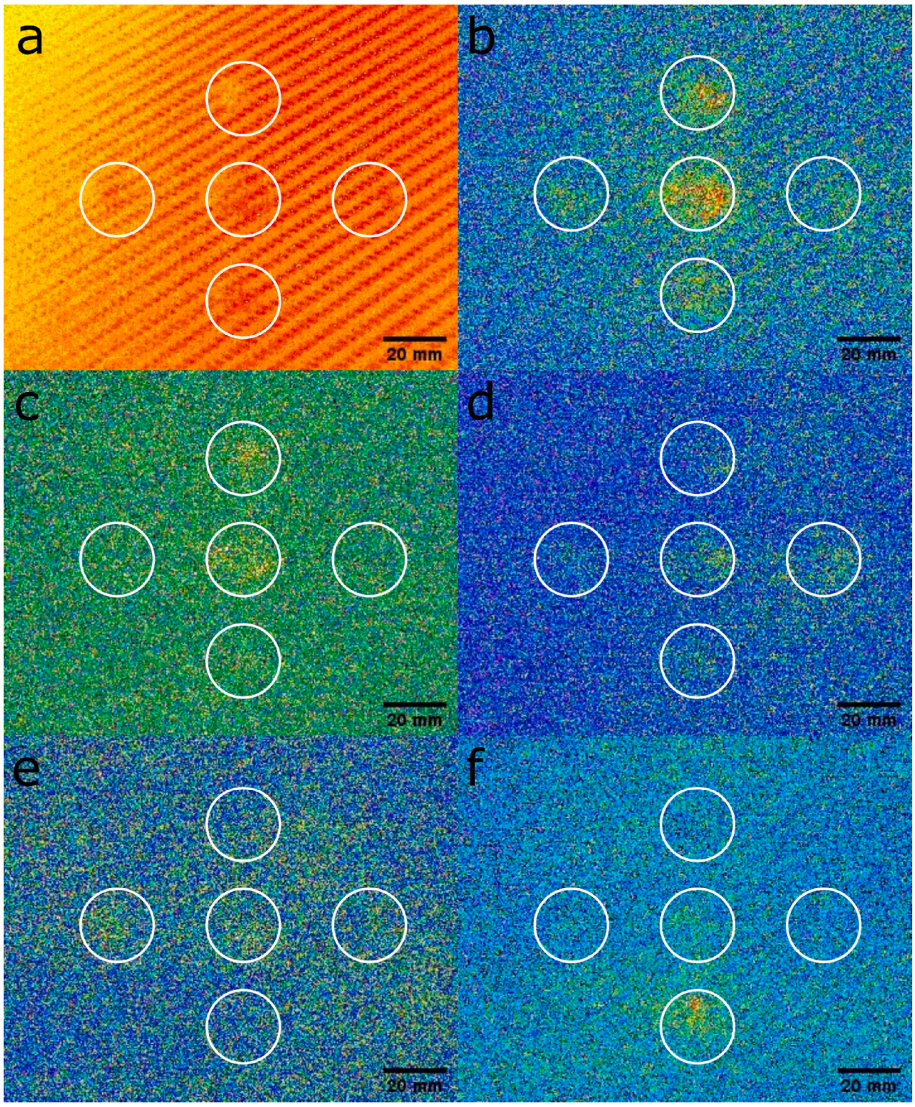

Fig. 10. Shows the apparent temperature difference increase for excitation of the sample shown in Fig. 1 (c). The white circles highlight the damage locations on the sample. (a) No excitation unprocessed image showing apparent temperature with the defects visible. (b) Excited at the centre (13.5 mm) defect. (c) Excited at the top centre (12 mm) defect. (d) Excited at the centre-right (6 mm) defect. (e) Excited at the centre-left (8 mm) defect. (f) Excited at the bottom centre (10 mm) defect. Red and yellow pixels indicate higher temperatures. (For interpretation of the references to colour in this figure legend, the reader is referred to the Web version of this article.)

focal region and the area immediately surrounding it, making them visible with an IR camera. This has been done and can be seen in Fig. 10 (c), (b) and (f) in sequence for a scan down the figure starting at the top with the excitation moving down.

A final set of measurements studied the sample with the 5 damage sites [Fig. 1(c)], with the array focussed on each of the damage locations. The range of damage sizes was from 6 to 13.5 mm in diameter. With the array focus located on each damage local heating for each can be observed in Figs. 10 and 11.

Fig. 9 shows that when the array focus is moved across the sample containing a range of damage sizes, a thermosonic response at each defect location is measured. It can be noted that with a 40 mm separation between the central defect and those surrounding it, some indications might be expected based on the results of Fig. 8. This is most clearly visible in Fig. 9(b), so that with excitation at the central damage, the surrounding damage locations also exhibit thermosonic heating. Excitation of the central defect can also be observed in Fig. 8 (c)–(f) when excited at the locations of the surrounding defects.

The sizes of the damage created with the varying sized ball bearings [Fig. 1(c)] vary significantly, with the 13.5 mm damage being more than double the size of the damage from the 6 mm ball bearing as shown in Fig. 1(c). Fig. 11 shows that despite the significant disparities in the size of the damage in the sample studied all of the damage locations show a similar level of heating for the same array conditions. This similar level of heating suggests that this method would allow even smaller defects to be identified with a similar level of thermosonically generated apparent temperature rise. With smaller damage locations the number of pixels experiencing a thermosonically generated apparent temperature rise would reduce and make them more difficult to detect and measure. As such smaller damage locations may require the camera to be focussed on a smaller area. This could be achieved by either locating the camera closer to the sample or the use of a more powerful zoom lens on the inspection to focus the IR camera more closely around the focal point to assist with identifying smaller defects with a greater number of excited pixels captured at the thermosonically-excited damage.

4. Conclusions

The application of a pulsed 40 kHz ultrasound signal from a commercially available air-coupled array applied to a damaged CFRP sample has resulted in thermosonic heating being observed. The level of the thermosonic response is dependent on both the distance from the damage at which the array is focused and the incident power from the array. This results in a reduced level of heating as the array focus is moved away from the damage location. The haptic array allows electronic control of the focal point of the array to scan it across the sample. This, in conjunction with IR imaging, will allow the detection of damage across a sample without contact. The need to make multiple measurements in many locations as is the current practice to cover an entire surface can be achieved with the use of an array to ensure all areas are inspected. This development allows the use of an air-coupled array source and IR camera to make an entirely non-contact measurement to determine if damage is present in a CFRP sample. This scanning ability could allow large areas to be investigated more rapidly and effectively than is currently possible. With Figs. 7 and 8 showing the increase in both the rate of apparent temperature rise and final apparent temperature change due to thermosonic excitation focus being closer to the damage or applying more ultrasonic power a larger and hence more powerful array would also assist in making smaller defects clearly visible.

These results showing that the damage shows localized heating with non-contact ultrasonic excitation at 40 kHz, which concurs with the existing literature on thermosonics. The use of an array source represents a significant development, with the electronic control of movement of the focal point across a sample being able to scan it and search for damage. Further development of this technique to enhance defect identification against the background noise in Figs. 5, 6 and 10 for both human and automated defect detection is being undertaken. For example, principal component analysis (PCA) - that is typically used for background noise removal of thermal data - and lock-in techniques are being investigated to achieve this."

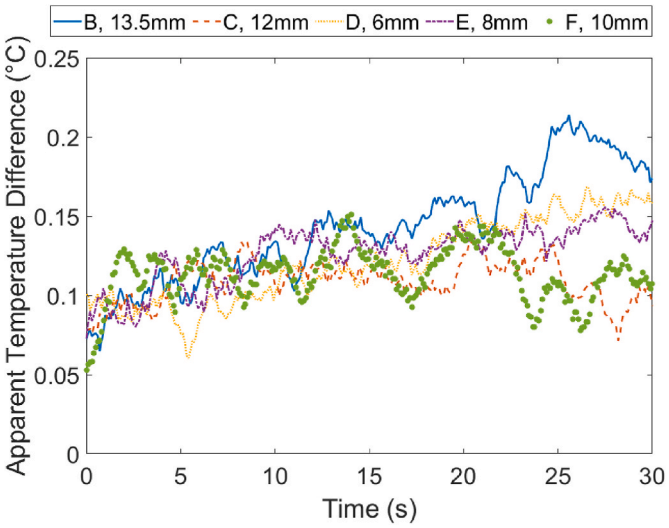

Fig. 11. A plot for the apparent temperature with respect to time for the focal points on the different sized defects presented in Fig. 9.

Author Statement

Richard Watson: Conceptualization, Methodology, Software, Investigation, Writing- Original draft preparation. Duncan Billson: Conceptualization, Methodology, Supervision, Writing - Review & Editing. David Hutchins: Writing- Reviewing and Editing. Francesco Ciampa: Conceptualization, Supervision, Project administration, Funding acquisition, Writing - Review & Editing.

Declaration of competing interest

The authors declare the following financial interests/personal relationships which may be considered as potential competing interests: FC reports equipment, drugs, or supplies and travel were provided by the Leverhulme Trust.

Acknowledgements

FC acknowledges the Leverhulme Trust, award RPG-2019-303, for supporting this research work. The authors would like to acknowledge the Engineering Build Space, Digital and Material Technologies Laboratory, Frank Courtney and Engineering workshops at the University of Warwick for use of their facilities and assistance with sample defect preparation. Authors finally acknowledge Mr Ashvin Jeyakumar who supported during the collection of thermal data.

References

[1] Heida JH, Platenkamp DJ. In-service inspection guidelines for composite aerospace structures. In: Proceedings of the 18th world conference on nondestructive testing, vol. 14; 2012.
[2] Marsh G. Airbus A350 XWB update. Reinforc Plast 2010;54:20–4. https://doi.org/10.1016/S0034-3617(10)70212-5.
[3] Chapter 7 - Defects and damage and their role in the failure of polymer composites. Greenhalgh. In: Emile S, editor. Woodhead publishing series in composites science and engineering, 'failure analysis and fractography of polymer composites'. Woodhead Publishing; 2009. p. 356–440. https://doi.org/10.1533/9781845696818.356.
[4] Baker AA, Jones R, Callinan RJ. Damage tolerance of graphite/epoxy composites. Compos Struct 1985;491:15–44. https://doi.org/10.1016/0263-8223(85)90018-2.

[5] Duchene P, Chaki S, Ayadi A, et al. A review of non-destructive techniques used for mechanical damage assessment in polymer composites. J Mater Sci 2018;53: 7915–38. https://doi.org/10.1007/s10853-018-2045-6.
[6] Ciampa F, Mahmoodi P, Pinto F, Meo M. Recent advances of active infrared thermography for non-destructive testing of aerospace components. Sensors 2018; 18(2):609. https://doi.org/10.3390/s18020609.
[7] Santos M, Santos J, Reis P, Amaro A. Ultrasonic C-scan techniques for the evaluation of impact damage in CFRP. Mater Test 2021;63(2):131–7. https://doi.org/10.1515/mt-2020-0020.
[8] Forsyth DS. Nondestructive testing of corrosion in the aerospace industry. In: [Corrosion control in the aerospace industry], 111–130; 2009. 9781845693459.
[9] Nagy Peter B. Fatigue damage assessment by nonlinear ultrasonic materials characterization. Ultrasonics 1998;36(1–5):375–81. https://doi.org/10.1016/S0041-624X(97)00040-1.
[10] Theobald P, Zeqiri B, Avison J. Couplants and their influence on AE sensor sensitivity. J Acoust Emiss 2008;26:91–7.
[11] Al-Khafaji SFA. The effect of coupling media on the pulse velocity of concrete". University of Leeds; 2017.
[12] Castaings M, Cawley P, Farlow R, Hayward G. Single sided inspection of composite materials using air coupled ultrasound. J Nondestr Eval 1998;17:37–45. https://doi.org/10.1023/A:1022632513303.
[13] Stoessel R, Krohn N, Pfleiderer K, Busse G. Air-coupled ultrasound inspection of various materials. Ultrasonics 2002;40:159–63. https://doi.org/10.1016/S0041-624X(02)00130-0.
[14] Maldague XPV. [Nondestructive evaluation of materials by infrared thermography]. Springer London, Limited; 1993. p. 1–22. https://doi.org/10.1007/978-1-4471-1995-1.
[15] Avdelidis NP, Hawtin BC, Almond DC. Transient thermography in the assessment of defects of aircraft composites" NDT&E International36; 2003. p. 433–9. https://doi.org/10.1016/S0963-8695(03)00052-5.
[16] Han X, Favro LD, Ouyang Z, Thomas RL. Thermosonics: detecting cracks and adhesion defects using ultrasonic excitation and infrared imaging. J Adhes 2001;76 (2):151–62. https://doi.org/10.1080/00218460108029622.
[17] Dionysopoulos D, Fierro GPM, Meo M, Ciampa F. Imaging of barely visible impact damage on a composite panel using nonlinear wave modulation thermography. NDT E Int 2018;95:9–16.
[18] Balageas D, Maldague X, Burleigh D, Vavilov VP, Oswald-Tranta B, Roche J-M, Pradere C, Carlomagno GM. Thermal (IR) and other NDT techniques for improved material inspection. J Nondestr Eval 2016;35:18. https://doi.org/10.1007/s10921-015-0331-7.
[19] Johnson DR, Chavez EL. Characterization of the thermosonic wire bonding technique. 1976. https://doi.org/10.2172/7353285 [Combination of ultrasonic energy and thermocompression]". United States: N. p.
[20] Fierro GPM, Ginzburg D, Ciampa F, Meo M. Nonlinear ultrasonic stimulated thermography for damage assessment in isotropic fatigued structures. J Sound Vib 2017;404:102–15.
[21] Tomlinson WJ, Winkle RV, Blackmore LA. Effect of heat treatment on the shear strength and fracture modes of copper wire thermosonic ball bonds to Al-1% Si device metallization. 3. In: IEEE Transactions on Components, Hybrids, and Manufacturing Technology, 13; 1990. p. 587–91. https://doi.org/10.1109/33.58864.
[22] Fierro GPM, Ginzburg D, Ciampa F, Meo M. Imaging of barely visible impact damage on a complex composite stiffened panel using a nonlinear ultrasound stimulated thermography approach. J Nondestr Eval 2017;36(4):69.
[23] Rantala J, Wu D, Busse G. Amplitude-modulated lock-in vibrothermography for NDE of polymers and composites. Res Nondestr Eval 1996;7:215–28. https://doi.org/10.1007/BF01606389.
[24] Favro LD, Han X, Ouyang Z, Sun G, Sui H, Thomas RL. IR imaging of cracks excited by an ultrasonic pulse. Proc. SPIE 4020 30 March 2000. https://doi.org/10.1117/12.381549. Thermosense XXII.
[25] Han X, Favro LD, Thomas RL. Detecting cracks in teeth using ultrasonic excitation and infrared imaging. Proc SPIE Biomed. Optacoustic. 15 June 2001. https://doi.org/10.1117/12.429316.
[26] Zalameda JN, Winfree JP, Yost WT. Air coupled acoustic thermography (acat) inspection technique. AIP Conf Proc 2008;975:467–74. https://doi.org/10.1063/1.2902697.
[27] Solodov I, Rahammer M, Derusova D, BusseG. Highly-efficient and noncontact vibro-thermography via local defect resonance. Quantitative InfraRed Thermography J 2015;12:98–111. https://doi.org/10.1080/17686733.2015.1026018.
[28] Culbertson H, Schorr SB, Okamura AM. Haptics: the present and future of artificial touch sensation. Annual Rev Control Robotic Autonomous Syst 2018;1(1): 385–409. https://doi.org/10.1146/annurev-control-060117-105043.
[29] Iwamoto T, Tatezono M, Shinoda H. Non-contact method for producing tactile sensation using airborne ultrasound. 08. In: inProc. 6th Int.Conf. Haptics: Perception, Devices Scenarios, ser. EuroHaptics; 2008. p. 504–13. https://doi.org/10.1007/978-3-540-69057-3_64.
[30] Hoshi T, Takahashi M, Iwamoto T, Shinoda H. Noncontact tactile display based on radiation pressure of airborne ultrasound. 3. In: IEEE Transactions on Haptics. 3; July-Sept. 2010. p. 155–65. https://doi.org/10.1109/TOH.2010.4.
[31] Neild A, Hutchins DA, Robertson TJ, Billson DR. Imaging using air-coupled polymer-membrane capacitive ultrasonic arrays. Ultrasonics 2004;42:859–64. https://doi.org/10.1016/j.ultras.2004.01.065.
[32] Watanabe A, Hasegawa K, Abe Y. Contactless fluid manipulation in air: droplet coalescence and active mixing by acoustic levitation. Sci Rep 2018;8:10221. https://doi.org/10.1038/s41598-018-28451-5.
[33] Zehnter Sebastian, Marco AB. Andrade and Christoph Ament, Acoustic levitation of a Mie sphere using a 2D transducer array. J Appl Phys 2021;129:134901. https://doi.org/10.1063/5.0037344.
[34] Ochiai Yoichi, Hoshi Takayuki, Rekimoto Jun. Three-dimensional mid-air acoustic manipulation by ultrasonic phased arrays. PLoS One 2014;9(5):e97590. https://doi.org/10.1371/journal.pone.0097590.